Quantifying syringeal dynamics *in vitro* using electroglottography

Jeppe H. Rasmussen[1], Christian T. Herbst[2], Coen P. H. Elemans[1,*]

[1] Department of Biology University of Southern Denmark, Denmark
[2] Department of Cognitive Biology, University of Vienna, Austria
* correspondence: coen@biology.sdu.dk

Keywords: Syrinx, birdsong, electroglottography, MEAD

Abstract

The complex and elaborate vocalizations uttered by many of the 10,000 extant bird species are considered a major driver in their evolutionary success, warranting study of the underlying mechanisms of vocal production. Additionally, birdsong has developed into a highly productive model system for vocal imitation learning and motor control, where, in contrast to humans, we have experimental access to the entire neuromechanical control loop. In human voice production, complex laryngeal geometry, vocal fold tissue properties, airflow and laryngeal musculature all interact to ultimately control vocal fold kinematics. Quantifying vocal fold kinematics is thus critical to understanding neuromechanical control of voiced sound production, but *in vivo* imaging of vocal fold kinematics in birds is experimentally challenging. Here we adapted and tested electroglottography (EGG) as a novel tool for examining vocal fold kinematics in the avian vocal organ, the syrinx. We furthermore imaged and quantified syringeal kinematics in the pigeon (*Columba livia*) syrinx with unprecedented detail. Our results show that EGG signals predict 1) the relative amount of contact between the avian equivalent of vocal folds and 2) essential parameters describing vibratory kinematics, such as fundamental frequency, and timing of syringeal opening and closing events. As such EGG provides novel opportunities for measuring syringeal vibratory kinematic parameters *in vivo*. Furthermore, the opportunity for imaging syringeal vibratory kinematics from multiple planar views (horizontal and coronal) simultaneously promotes birds as an excellent model system for studying kinematics and control of voiced sound production in general, including humans and other mammals.

INTRODUCTION

Birds produce a wide variety of sounds crucial to their survival and communication (Marler and Slabbekoorn, 2004). Additionally, birdsong has developed into an important model system to study motor sequence learning (Fee and Scharff, 2010) and imitative vocal learning in humans (Brainard and Doupe, 2013; Doupe and Kuhl, 1999). Birdsong is a highly quantifiable stereotyped behaviour, which, combined with discrete neural substrates, promotes understanding of links between brain and behaviour (Bolhuis and Gahr, 2006; Brainard and Doupe, 2013). Despite the fact that mammals and birds use two different vocal organs, the larynx in mammals and the syrinx in birds, we recently demonstrated that the same physical mechanism underlies their voiced sound production, i.e., the myoelastic-aerodynamic mechanism (Elemans et al., 2015; Titze, 1980; Titze, 1994; Van den Berg, 1958). This finding constitutes yet another parallel between the motor control of voiced sound production and allows us to exploit the much larger literature on human voice production and its control to further our understanding of vocal production and control in birds, and potentially vice-versa.

The neuromechanical control of voiced sound production is formed by a closed-loop, of which the neural circuitry (brain) and biomechanics (sound production and perception) form an integral part (Düring and Elemans, 2016; Goller and Riede, 2013; Suthers and Margoliash, 2002). To fully comprehend the motor control of sound production, we thus need to understand both neural mechanisms as well as peripheral biomechanics. In birds, great advances have been made in elucidating the activity of individual neurons involved in their vocalization (Berwick et al., 2011; Keller and Hahnloser, 2009; Markowitz et al., 2015) and neuromechanical control models (Amador et al., 2013). However we have little quantitative data on the peripheral biomechanics in avian sound production that are essential to interpret neural signals and validate models (Düring and Elemans, 2016; Goller and Cooper, 2004; Riede and Goller, 2010; Zollinger and Suthers, 2004).

In humans, the physical and physiological framework of laryngeal sound production for speech and singing has been relatively well described. The cyclical motion of the vocal folds periodically obstructs the passage of respiratory air, leading to pressure fluctuations in the vocal tract that are radiated as sound (Story, 2002). The complex laryngeal geometry, vocal fold tissue properties, airflow and musculature all interact to ultimately control the kinematics of the vocal folds (Herbst et al., 2011; Herbst et al., 2009; Titze and Talkin, 1979), thus causally influencing the radiated sound. The quality of the cyclical motion of the vocal folds determines, amongst others, the fundamental frequency (f_o) and the spectral slope (Alipour et al., 2012) of the generated sound, equally relevant for speech communication and singing (Herbst et al., 2015). Because of the critical role in setting important acoustical cues during voice production in both healthy and pathological voice production, quantifying and analysing vocal fold motion is and has been a main research focus for several decades in humans. Quantifying syringeal vibratory kinematics must likely be equally essential for explaining vocal variation in birds. However we currently lack detailed quantitative insight into syringeal vibratory kinematics.

Ideally, we would like to be able to quantify the time-varying 3D geometry of the syrinx at high speed during sound production *in vivo*. However, quantifying the motion of the avian equivalent to mammalian vocal folds, the lateral labia and medial labia in songbirds (Düring et al., 2013; Goller and Larsen, 1997b) and the lateral vibrating masses (LVM) in non-songbirds (Elemans et al., 2008) is experimentally difficult due to the small size and anatomical location of the syrinx deep in the body. Endoscopic high-speed imaging has been used successfully (Goller and Larsen, 1997a; Jensen et al., 2007), but remains very challenging in anaesthetized birds, let alone in freely singing birds. Another approach for imaging syringeal dynamics is using an *in vitro* (Fee et al., 1998; Paulsen, 1965), or perfused whole organ approach *ex vivo* (Elemans et al., 2015). However we have insufficiently detailed knowledge regarding syringeal motor control to meaningfully mimic song *ex*

vivo. It is thus critical to gain detailed insight into the syringeal vibratory kinematics *in vivo* and how this affects vocal production.

A less intrusive technique to investigate *in vivo* vocal fold dynamics in humans is electroglottography (EGG), which measures the variation in impedance between two electrodes, placed on the thyroid cartilage on each side of the vocal folds. Because air is a much better insulator than tissue, the impedance will depend on how much contact there is between the vocal folds (Rothenberg, 1992; Titze, 1990). An AC current with a frequency of 2 MHz is used to overcome the relatively nonconductive layer of skin and the myelin insulation of muscle fibres between the vocal folds and the electrodes (Rothenberg, 1992). The EGG signal has been shown to correlate well with the time-varying relative vocal fold contact area (rVFCA), which is the area of contact between the two vocal folds (Hampala et al., 2015; Scherer et al., 1988), but cannot predict either the absolute VFCA (Hampala et al., 2015) or lateral vocal fold displacements.

Here we test whether EGG can be used to quantify essential parameters for describing syringeal kinematics, such as fundamental frequency (f_o) and timing of opening and closing events, and thus whether EGG could be used as a viable tool for examining syringeal dynamics *in vivo*. We recently established paradigms to study sound production *in vitro* (excised) and *ex vivo* (perfused whole organ), which allows for new opportunities to image syringeal kinematics at high temporal (<25,000 fps) and spatial resolution (~5-30 µm) from different orientations simultaneously (Elemans et al., 2015). Using this approach we can image and quantify syringeal vibratory kinematics in unprecedented detail, which allows us to test alternative methods to direct imaging for quantifying syringeal vibratory kinematics that may be applicable *in vivo*.

MATERIALS AND METHODS

Specimens. Previous work observed syringeal dynamics with high imaging quality in domestic pigeons (Elemans et al., 2015). Therefore we examined the syringes of 8 adult male domestic pigeons (*Columba livia*) that were kept in a 3 x 6 x 2 m outdoor aviary at the University of Southern Denmark with food and water *ad libitum*. All procedures were carried out in accordance with the Danish Animal Experiments Inspectorate (Copenhagen, Denmark).

Surgical procedures. The birds were collected in the aviary in an opaque box to minimize the stress for the animal. In order to avoid blood clotting in the syrinx the animal was injected IM with 80 µl/kg bodyweight of 5000 units/ml Heparin (Amgros, Denmark) using a 30G needle on a Hamilton 50 µl syringe 30 minutes prior to the experiment. Animals were euthanized by isoflurane (Baxter Medicals, IL, USA) overdose. An incision was made 2-3 mm left of the sternum. The ribcage was opened, the bronchi were cut as close to the lungs as possible, and the trachea was cut about 10 cm cranial of the syrinx.

The syrinx was extracted and placed in oxygenated Ringer's solution (recipe as in (Elemans et al., 2004)) in a Sylgard covered petri dish on ice. The syrinx was cleaned of blood and excess adipose tissue and mounted in the experimental chamber (see below), ventral side up. The bronchi were tied airtight onto silastic tubing using 5.0 monofilament sutures (Argos surgical instruments, Newport Beach, CA, USA). The trachea was fastened airtight onto a custom-made plastic connector using 4.0 sutures (Argos surgical instruments, Newport beach, Ca, USA). Two EGG electrodes were fixed with 10.0 monofilament suture (Argos surgical instruments, Newport beach, Ca, USA) bilaterally onto tracheal ring T1.

Experimental chamber design and hardware. We used an *in vitro* paradigm to study sound production as described in detail in (Elemans et al., 2015). In brief, the excised syrinx was placed in an airtight chamber that allowed for precise control of air pressure, flow, humidity and temperature. The air pressures in the chamber and bronchi were controlled by two dual valve differential controllers (model PCD, Alicat Scientific Inc., Az, USA) with a 0-10 kPa gauge pressure range. The flow through the bronchi was measured using a flow transducer (model PMFc3000 Posifa Microsystems, San Jose, USA; 3 standard litres per minute full scale, response time 1 ms). Care was taken to mount the syrinx in its natural position. Because in pigeons the LVMs are attached to and encased by the rigid ossified skeleton of the syrinx, LVM adduction and tension is not affected as a result of incorrect mounting. Instead LVM tension is affected by the differential pressure between airsac and bronchus (termed transmural pressure) (Elemans et al 2008), and syringeal muscles (Elemans et al 2004; 2006). The pressure difference is carefully controlled for in the experiments as described in detail below. This situation is in contrast with excised larynx experiments where mounting requires assumptions on vocal fold adduction, length, edge approach and position symmetry that critically affect the conditions for vibration.

The experimental chamber had a glass lid allowing imaging of the syrinx in the coronal plane with a high-speed CMOS camera (model HS4, IDT) through a stereomicroscope (Leica, M165 FC, Leica Microsystems, Germany). This camera could capture up to 5000 fps at full frame image size of 1024x1024 pixels. Below the syrinx the experimental chamber had a glass window to allow transillumination of the syrinx by a 1700 lumen white LED powered by a stable power source (PS23023, HQ Power, Belgium). To image the syrinx from a tracheal perspective (the horizontal plane) we used either the HS4 camera or a videokymographic (VKG) camera (model 2156, Cymo B.V., Holland) (Qiu and Schutte, 2006) through a 1.2 mm diameter flexible endoscope (Scholly

Germany). The VKG system combined a CMOS chip capturing at 25 Hz full-frame in colour and a monochrome line-scan camera capturing a centred horizontal line at 7.2 kHz.

Sound pressure was measured in between 2-4 cm distance (accuracy ±1 mm) from the tracheal tube outlet with a ½ inch condenser microphone (model 40AF with preamplifier type 26AH, G.R.A.S. Denmark). The microphone signal was amplified (model 12AQ, G.R.A.S., Denmark) and system sensitivity was calibrated prior to each experiment with a microphone calibrator (model 42AB, G.R.A.S., Denmark).

EGG signals were recorded using a modified two-channel EGG device (model EG2, Glottal Enterprises Inc. NY, USA) (Rothenberg, 1992). In contrast to the three cm diameter gold plated disc electrodes placed on human skin (Rothenberg, 1992; Scherer et al., 1988), we used wire electrodes attached directly on the vibrating tissue as in (Elemans et al., 2015). The electrodes consisted of 28 µm Formvar insulated nichrome wire (A-M systems, USA) soldered to a four-pin connector connected to airtight electrical connectors inside the experimental chamber. Due to the higher vibration frequencies expected in birds (f_o is typically 500 – 5000 Hz) compared to humans, the frequency response of the EG2 device was extended upwards by the manufacturers (M. Rothenberg and M. Lyaski). Additionally, because trial runs showed that the EGG signals on the syrinx with our electrode design exceeded 20V peak-to-peak, the EGG device was modified allowing reduced amplification settings. Two additional three-position switches allowed individually changing the frequency ranges and amplification of each channel from the standard low-pass filter setting on the device (LF) up to either 10 kHz, 12 kHz, or 13.5 kHz, with concurrent amplification settings of 1x, 1/2x and 1/3x respectively.

Data acquisition and synchronization. All data-acquisition, data-analysis and control software was custom-written in Matlab. A 1 ms TTL trigger pulse was generated to synchronize recordings and to trigger the HS4 highspeed camera. Pressure, flow, trigger and audio signals were low-pass filtered with a cut-off frequency of 10 kHz (custom build filter Thor labs, Newton, New Jersey, USA) and digitized with a 16 bit AD converter (NI USB 6259, National Instruments, Austin, USA) at a sampling frequency of 48 kHz and saved as binary files in Matlab's MAT format (Mathworks, Natick, Ma, USA). The microphone signal was corrected for delay due to the velocity of sound in air with respect to the other recorded signals. The analogue video output from the VKG was digitized with an audio-video capturing device (Intensity Extreme, Black Magic Design Pty Ltd, Australia) together with the microphone and trigger signals (on the two respective audio channels) and saved as AVI files. We recorded data with three separate systems, i.e. the VKG, the digitized signals, and the HS4 camera, resulting in three different file data-streams. To synchronize the data stream of these systems in time, we measured the three time delays in our system: 1) time delay *d1*: an intrinsic delay in the VKG system between the video and audio signal by design of the VKG system, 2) time delay *d2*: time between triggers in the VKG AVI file time and MAT file, 3) time delay *d3*: intrinsic delay between trigger and capture of the high-speed camera. Delay *d1* was determined prior to experiments for each subject. A LED was connected to the trigger signal and filmed with the VKG system and high-speed camera. The synchronization runs consisted of 4 consecutive frequency sweeps (40 to 1000 Hz) of a 1ms wide TTL signal. To determine *d1*, we calculated the cross correlation between the audio channel on the AVI file and the intensity value of the LED filmed by the VKG. The averaged time delay *d1* was 42.2 ± 3.7e-3 ms (N=47). Delay *d2* was measured for each recording as the time difference between trigger onsets on AVI and MAT files. Delay *d3* was determined prior to experiments. We imaged the intensity of the LED sync signal described above with the high-speed camera at 48 kHz and cross-correlated the sync signal

with the light intensity signal. No delay more than one image frame duration (i.e. 21 µs) was detected.. Because *d3* measured less than 21 µs, we did not correct for this delay.

Experimental protocol. We induced phonation by ramping up bronchial pressure (p_b) from 0 to 3 kPa at a speed of 1 kPa/s, at the same time applying constant pressure in the experimental chamber, analogous to the interclavicular air sac pressure (p_{ICAS}) of 1 kPa. These pressure values are physiologically realistic for Ring doves (Beckers, 2003; Elemans et al., 2008) and were used previously to reliably induce self-sustained vibrations in domestic pigeons (Elemans et al., 2015). We first imaged LVM vibrations in the horizontal plane (endoscopically through the trachea) with the full frame high-speed camera at 3000 fps. To facilitate automatic extraction of the glottal opening area in this orientation we placed a light source caudally to the LVM, in order to enhance the contrast between the LVM tissues and opening in between. Secondly, we simultaneously imaged the LVM vibrations in the coronal plane with the high-speed camera (by transillumination) and in the horizontal plane (endoscopically) with the line-scan camera at 7200 Hz during a pressure ramp (p_b =0-3 kPa @ 1kPa/s, p_{ICAS}=1 kPa). It was experimentally challenging to achieve the correct lighting conditions allowing LVM extraction in both coronal and horizontal plane simultaneously. Out of 8 individuals, we were able to generate high quality data in 3 animals that were used for further analysis.

Contact area. In laryngeal voiced sound production the EGG signal relates to the relative vocal fold contact area (rVFCA). Because the sound producing vibrating structures in birds (i.e. LVMs) are not termed vocal folds, we will use the abbreviation LVMCA in this manuscript. To verify the physiological relevance and reliance of the EGG signal in birds we estimated LVMCA from our combined endoscopic (horizontal plane) and transillumination (coronal plane) imaging data (Fig 1).

First, we investigated the presence of dorsoventral (DV) LVM waves in the horizontal plane using the tracheal endoscopic view. We extracted the lateral distance between the two LVMs as a function of DV position and time (Fig. 2) a.k.a. glottovibrogram (Karakozoglou et al., 2012; Lohscheller and Eysholdt, 2008). To determine if opening/closing events travelled as a wave we calculated the normalized distance between the LVMs for all DV positions as a function of the phase of the cycle (Fig. 2C). We calculated a linear regression of the phase at maximal opening across the DV positions (Fig. 2D), which relates to the speed v of a travelling in the DV direction. As imaging was done simultaneously in the coronal plane and the horizontal plane we could use structures seen in both planes to calibrate the endoscopic view from the calibrated coronal view.

Second, we investigated LVM contact area in the coronal plane using the transilluminated view. Obtaining high quality transillumination imaging with clearly visible LVMs was very sensitive to lighting conditions, and we included only experimental runs where the LVMs were easily seen. Even so automatic extraction of LVM shape was not possible and therefore we manually scored caudal-cranial contact between the two LVMs. To calculate the caudo-cranial height of tissue contact (H), we visually determined the most cranial and most caudal point of contact between the LVMs in 580 frames of 30 oscillations.

LVMCA was approximated as the product of H and the DV length (L) of the LVM. As the contact between the LVMs results from the transillumination projection, we use the term *projected* LVM contact area (pLVMCA). Ten consecutive cycles were investigated from 3 specimens (at p_{ICAS}=1 kPa, p_b =2 kPa). Furthermore we calculated the closed quotient for these cycles from the pLVMCA signal as the ratio between the duration the syrinx was closed (i.e. pLVMCA >0) and the duration of the entire cycle. To avoid observer bias regarding correlation to EGG, the observer was not able to see the synchronized EGG signal during this scoring process.

In human laryngeal EGG analysis, the changes in value of the EGG signal, i.e. the first derivative of the EGG signal (dEGG), are often used to approximate key events within a vibratory cycle where contact between the paired vibrating vocal fold tissue is gained or lost (Childers and Krishnamurthy, 1985; Herbst et al., 2014). Therefore we extracted both maxima and minima of the dEGG signal for each of the 10 analysed vibratory cycles per specimen.

***f_o* extraction from EGG and LVM motion.** To extract the fundamental frequency of LVM vibrations in the coronal plane we computed digital kymograms (DKG) from the high-speed imaging data to observe periodicity in the vibrations (Harm K. Schutte et al., 1998; Švec and Schutte, 1996). From the DKG we extracted the LVM vibration period and thereby the frequency, of the LVM. The f_o of the EGG signal was extracted using autocorrelation.

Wavegram visualization of EGG signals. To be able to follow the development of the EGG waveform representing within-cycle vibration kinematics during dynamic pressure ramps, we constructed wavegrams of the EGG signals (Herbst et al., 2010). In brief, a wavegram isolates individual cycles of the EGG or dEGG signal and normalizes the duration and amplitude of each

cycle. The time-varying normalized signal amplitude within each individual cycle is then colour coded. The resulting strips of pixels are consecutively aligned from bottom to top along the y-axis, where the position on the x-axis represents the respective time coordinate (i.e., overall time is mapped onto the x-axis), and the position of the y-axis represents normalized intra-cycle time.

Statistics. No sample sizes were computed before the experiments. A technical replicate is a replicate of the measurement on the same preparation, and a biological replicate is an individual. Data are presented as mean values ± 1 SD. No outliers were excluded.

RESULTS

Testing the EGG technique required measuring the contact area between the vocal folds (vocal fold contact area, VFCA). Previously we imaged the inner edges of the lateral vibratory mass (LVM) in the pigeon syrinx during self-sustained vibrations using transillumination (Elemans et al., 2015). This technique allowed us to look through the tissue, analogous to an x-ray image. Because this technique resulted in a projected image, motion and different positions of the LVM perpendicular to the coronal plane are superimposed and thus averaged in the coronal projection. This may lead to 1) a decreased precision of the LVM position in the coronal projection, but also to 2) an oversimplification of the physical processes at play as we would miss the presence of DV waves. Establishing the presence of DV waves is thus essential to better understand the physical progresses but also to increase the accuracy of the LVM positioning and estimation of LVMCA.

Dorsoventral syringeal vibrations

Therefore we first tested the presence of DV oscillatory modes during sound production. We induced sound production in the syrinx of domestic pigeons *in vitro* and quantified LVM vibration dynamics in the horizontal plane using tracheal endoscopic high-speed imaging in 588 opening/closing events in 3 different animals (Fig 2). To detect phase differences along the DV axis we measured the distance between the LVMs within each oscillatory cycle along the DV axis (Fig 2C) and regressed the phase of the maximal LVM distance relative to the maximal opening at midline along the DV axis (Fig 2D). If the LVMs would open for example in a zipper-like mode as sometimes observed in humans (Hess and Ludwigs, 2000) and elephants (Herbst et al., 2013), the maximal opening would shift in phase along the DV axis.

Over a range of vibration frequencies, the maximum phase delay did not exceed 1.2 deg/mm (length of LVM = 5.0±0.2 mm) and was <0.8 deg/mm for 95% of all openings in all animals (Fig. 2). The peak of the normal distribution was 0.083±0.15, 0.22±0.19 and 0.07±0.53 deg/mm for the three animals, respectively. Concluding, our data show that the projected inner surface of the LVMs represents LVM phase in the coronal projection within 0.8 deg/mm for 95% of all openings. Furthermore our data show that at any point along the DV axis the LVMs moved in phase. Therefore DV travelling waves were considered to be not present.

EGG as a predictor of LVM vocal fold contact area

Because DV waves were absent, we estimated the LVMCA from the coronal projection alone and did this over ten consecutive oscillatory cycles in three animals (Fig 3). The projected LVMCA (pLVMCA) changed magnitude consistently within the oscillatory cycle for all three individuals. LVMCA sharply increased after glottal closure up to a maximum pLVMCA of 10.7 ± 0.6 mm^2

(N=3 animals) (range: 10.2 - 11.3 mm^2) at 0.6±0.1 ms (range: 0.49 - 0.71 ms) after first contact of the LVMs. The closed quotient (part of the oscillation where the syrinx is closed as determined by transillumination) was not significantly different between individuals (one-way Anova, p= 0.402) and measured 0.47±0.03 (N=3, raw data: 0.47±0.02, 0.46±0.03, 0.48±0.03 (N=10 technical replicates) for the three biological replicates respectively).

Next we tested whether the electroglottography (EGG) technique can predict essential parameters quantifying syringeal kinematics such as LVMCA, timing of opening and closing events, and fundamental frequency (f_o), and thus whether EGG can be ultimately used as a viable tool for examining syringeal dynamics *in vivo*. The overall shape of the pLVMCA and EGG signal consisted of a steep increase at first contact followed by a variable decrease until complete loss of contact between the LVMs in all three animals (Fig 3ACE), but their relative differences over the entire vibration cycle varied between -44% and 76% (Fig 3BDF). At LVM closure, first contact between the LVM was associated with a sharp increase in the EGG signal (in these examples within 0.6 ms) and a peak in the derivative of the EGG signal (dEGG) occurred at -0.10±0.10, -0.12±0.09 and 0.61±0.12 ms (N=10) after contact for the three animals, respectively. At LVM opening, we observed a time difference between the opening event and the minimum dEGG of -1.45±0.14, -0.89±0.11 and 0.48±0.27 ms, respectively. From these values we computed contact quotients (part of the oscillation where the syrinx is hypothesized to be closed, based on the EEG signal) of 0.24±0.01, 0.47±0.02 and 0.40±0.01 (N=10) for the three animals, respectively.

Previous research in a canine excised larynx revealed that the dEGG minima and maxima do not precisely coincide with the events of glottal opening and closure (Herbst et al., 2014), corroborating the notion that glottal closure and opening constitute different physiological events than vocal fold contacting and decontacting (Herbst et al., 2017b). It is therefore not surprising that a number of different algorithms for (arbitrarily) defining the (de)contacting events within the EGG signal have

been suggested. In one of those, the opening event in the EGG signal has been defined arbitrarily as the time where the normalized VFCA has dropped to 3/7 of its max value within a cycle (Howard, 1995; Howard et al., 1990). This criterion is met -1.10±0.19, -0.13±0.09 and 0.23±0.26 ms after opening, for the three animals respectively, thus leading to an improvement of 0.25 to 0.76 ms compared to the dEGG concept. Using the 3/7 approach resulted in contact quotients of 0.32±0.01, 0.46±0.01 and 0.43±0.01 (N=10) for the three animals, respectively.

EGG as a predictor of LVM f_o

Next we tested whether the EGG signal can predict the oscillatory frequency of the LVMs, by extending our analysis using digital kymographs that visualize multiple vibrations (Fig 4). We measured the elapsed time between consecutive closing events on digital kymograms and EGG peaks (Fig 4BC) over a range of f_o values resulting from different bronchial pressure excitations. The data show a very strong correlation between the fundamental frequency of the EGG signal and the oscillatory frequency of the LVMs (slope = 0.9603, 0.9889 and 0.8786 and R^2=1.0, 1.0 and 0.8775 for the three animals respectively, and R^2= 0.991 for all animals combined) (Fig 4D).

EGG as a predictor of oscillatory modes

Taken together, the EGG signal fairly accurately predicted several landmark events in the LVMCA oscillatory cycle of the LVMs, such as f_o and syringeal closure. Building on these findings, we followed the development of the EGG signal over time during a dynamic phonation situation using wavegrams (Herbst et al., 2010) (Fig 5). We subjected the syrinx to a p_b ramp from 0 to 2 kPa (1 kPa/s ramp speed) at constant air sac pressure of 1 kPa. This quasi-steady excitation resulted in a range of oscillatory frequencies from 80 to 160 Hz. The wavegram of one individual suggested that two vocal modes were present with distinct EGG wave shapes (Fig 6): mode 1 was

present when transmural pressure was <0.3 kPa from the phonation onset to 1.5 seconds into the run and also from 2.8 s to the end, and mode 2 was present in between when transmural pressure was >0.3 kPa . The *fo* ranged from 70 to 125 Hz and 125 to 150 Hz for mode 1 and 2 respectively. We confirmed the existence of distinct syringeal oscillatory modes using our endoscopic imaging data of LVM motion (Fig 6F). Distinctly different modes were observed with contact quotients of 0.94 and 0.72 for mode 1 and 2 respectively.

DISCUSSION

We show that electroglottography can be used to estimate syringeal vibratory kinematics in birds *in vitro*. The relative LVMCA is followed within a cycle, leading to accurate predictions of LVM vibration f_o, and to approximation of landmark events, such as syringeal closing and opening event timing, during sound production in pigeons. Determining the timing of opening events from the EGG signal improved by using different combinations of dEGG and EGG signal magnitudes as also used in human EGG studies (Howard, 1995; Howard et al., 1990). However, in analogy to what has been shown for humans (Echternach et al., 2010; Herbst et al., 2017b; Lã and Sundberg, 2015), without rigorous experimental validation as presented here care should be taken when presenting contact quotients (Herbst et al., 2017b) based on the EGG signal alone. Furthermore, investigation with a larger number of syringes, potentially from different species, is required to determine which algorithm for estimating the EGG contact quotient best matches the respective closed quotients. The distinction between EGG contact quotient and closed quotient is essential, because only the latter has a true causal relation to the laryngeal and syringeal sound generation events.

Compared to EGG signals from the human larynx, we do not observe a baseline during the part of the cycle without tissue contact (Rothenberg, 1992; Scherer et al., 1988). Furthermore we observed additional smaller peaks in both EGG and dEGG signals. Firstly, these disparities could arise from phase distortions within the acquired signal. Secondly, the phenomenon could be in part due to differences in electrode design and placement in birds versus humans (3 cm diameter gold plated disc electrodes placed on the neck versus 26 µm diameter wire NiChrome electrodes placed directly on the LVMs) and variation in electrode placement between individuals. For the EGG signal to be linear and unbiased, the electric field lines between the electrodes must have uniform density across the area of interest. This is accomplished in humans by having electrodes of a size not smaller than the area wherein the tissue collisions happen (Titze, 1990). In our experiments the electrodes were located caudo-cranially, close to where the first contact happens during a cycle (Elemans et al., 2015). During the cycle the caudo-cranial location of tissue contact moves cranial before the decontacting event. This means that the electric field lines will have a higher density at the location of contact than at the location of decontacting. Placing the EGG electrodes further away from the syrinx and increasing the size of the electrodes to improve linearity of the EGG signal is unfortunately not possible as the syrinx *in vivo* is suspended in air inside the interclavicular air sac. Thirdly, not only the LVMs are oscillating during sound production in pigeons, but also the medial tympanic membranes (MTM). These thin structures are located caudally to the LVMs on the medial side of the primary bronchi, stretching caudally from the pessulus (Goller and Larsen, 1997a; King, 1989). Future studies may evaluate if and how their vibrations affect the shape of the EGG signal.

Furthermore we show that distinct EGG waveforms in the wavegrams reflected distinct vibratory regimes, which implies that the EGG signal has the potential to detect distinct vibratory regimes of the LVMs. The transmural pressure in pigeons during sound production has not been directly measured *in vivo*. However, measurements and models (Beckers, 2003; Elemans et al., 2008) suggest that transmural pressures of 1-2 kPa during dynamic vocal situations are possible in ring doves, a close relative to the pigeon. Driving the syrinx with this physiologically reasonable pressure range, we were able to induce LVM vibrations from about 50 to 250 Hz. LVM dynamics showed two distinct vibratory modes in this range, potentially analogous to different laryngeal mechanisms in humans (Henrich, 2006). The f_o range for domestic pigeon vocalization is 150-400 Hz (Goller and Larsen, 1997a). This range suggests that pigeons primarily use the 2nd observed oscillatory regime (f_o >125-Hz) - a hypothesis that remains to be tested *in vivo*. In support of this notion, it seems physiologically reasonable that pigeons have both or more oscillatory regimes at their disposal *in vivo*, and comparable modes has also been observed in anesthetised crows (Jensen et al., 2007).

The unique possibility of visualising LVM shape by transilluminating the pigeon syrinx, together with the absence of dorsoventral LVM waves, allowed us to quantify LVMCA for the first time in birds. The syringeal LVMCA waveform in pigeons demonstrates several similarities to laryngeal VFCA measurements. First, as in the human and canine larynx, a sharp increase in the amount of tissue contact follows initial contacting (Boessenecker et al., 2007; Doellinger and Berry, 2006; Herbst et al., 2014). Just as observed here, the maximal tissue contact is reached within 1 ms after initial tissue contact. In the three animals investigated here we find similar pLVMCA waveforms within the oscillatory cycle and peak values of around 11 mm^2 (with H = 2.2 mm and DV length = 5.0 mm). Second, we find closed quotients of around 0.7, which is at the upper limit of what is found in humans and dogs (Herbst et al., 2009; Howard et al., 1990; Verdolini et al.,

1998a; Verdolini et al., 1998b), but below values of 0.82 measured in an elephant larynx (Herbst et al., 2013). In addition to the data presented here, only very few measurements of absolute VFCA have been reported. To our knowledge there are no absolute VFCA measurements reported for human vocal folds, but only for dogs (Gunter, 2003; Jiang and Titze, 1994). Different techniques have been used to determine VFCA in dogs and deer (Hampala et al., 2015; Herbst et al., 2017a; Jing et al., 2017; Shau et al., 2001). However, because we can image LVM dynamics simultaneously from different angles, birds provide an excellent model system to study the kinematics and control of voiced sound production.

Summarizing, we think that EGG could be a promising tool for predicting essential motion parameters of syringeal vibration in birds *in vivo*. Here, we studied syringeal vibratory kinematics in pigeons *in vitro*, which allowed for the quantification of LVMCA. This approach will be more challenging in small songbirds, such as zebrafinches, where imaging using tracheal endoscopy resulted in lower spatial and temporal resolution and was experimentally challenging even *in vitro* and the dense syringeal musculature limits transilluminating the syrinx for observing caudocranial waves (Elemans et al., 2015). Nevertheless, we think that EGG can be an interesting alternative to e.g. bronchial flow measurements for investigating song lateralization of the two individually controlled sound generators in songbirds. Also, by combining EGG measurements with phenomenological or simplified lumped-mass models, as regularly done in humans (Ishizaka and Flanagan, 1972; Story and Titze, 1995) it may be possible to infer other critical data such as vocal fold position and shape, larynx position, and even muscle activation to assess syringeal motor control.

Competing financial interests

The authors declare no competing financial interests.

Corresponding authors

Correspondence to: Jeppe Have Rasmussen (jeppehave@gmail.com) and Coen Elemans (coen@biology.sdu.dk)

Author contributions

JHR & CPHE developed the concepts and designed experiments. JHR performed all experiments. All authors participated in software development and data analysis. JHR prepared the figures. JHR & CPHE wrote first draft of the manuscript. All authors edited the manuscript and approved the final version.

Funding

This research has been supported by Danish Research Council (FNU) and Carlsberg Foundation grants to CPHE and an ‘‘APART’’ grant received from the Austrian Academy of Sciences to CTH.

References:

Alipour, F., Scherer, R. C. and Finnegan, E. (2012). Measures of spectral slope using an excised larynx model. *Journal of Voice* **26**, 403-411.

Amador, A., Perl, Y. S., Mindlin, G. B. and Margoliash, D. (2013). Elemental gesture dynamics are encoded by song premotor cortical neurons. *Nature* **495**, 59-64.

Beckers, G. J. L. (2003). Mechanisms of frequency and amplitude modulation in ring dove song. *Journal of Experimental Biology* **206**, 1833-1843.

Berwick, R. C., Okanoya, K., Beckers, G. J. and Bolhuis, J. J. (2011). Songs to syntax: the linguistics of birdsong. *Trends in cognitive sciences* **15**, 113-121.

Boessenecker, A., Berry, D. A., Lohscheller, J., Eysholdt, U. and Doellinger, M. (2007). Mucosal Wave Properties of a Human Vocal Fold. *ACTA ACUSTICA UNITED WITH ACUSTICA* **Vol. 93**, 815–823.

Bolhuis, J. J. and Gahr, M. (2006). Neural mechanisms of birdsong memory. *Nature Reviews Neuroscience* **7**, 347-357.

Brainard, M. S. and Doupe, A. J. (2013). Translating birdsong: songbirds as a model for basic and applied medical research. *Annu Rev Neurosci* **36**, 489-517.

Childers, D. G. and Krishnamurthy, A. K. (1985). A critical review of electroglottography. *Critical reviews in biomedical engineering* **12**, 131-161.

Doellinger, M. and Berry, D. A. (2006). Visualization and quantification of the medial surface dynamics of an excised human vocal fold during phonation. *Journal of Voice* **20**, 401-413.

Doupe, A. J. and Kuhl, P. K. (1999). Birdsong and human speech: Common themes and mechanisms. *Annual Review of Neuroscience* **Vol 22**, 567-631.

Düring, D. N. and Elemans, C. P. (2016). Embodied motor control of avian vocal production. In *Vertebrate Sound Production and Acoustic Communication*, pp. 119-157: Springer.

Düring, D. N., Ziegler, A., Thompson, C. K., Ziegler, A., Faber, C., Muller, J., Scharff, C. and Elemans, C. P. (2013). The songbird syrinx morphome: a three-dimensional, high-resolution, interactive morphological map of the zebra finch vocal organ. *BMC Biol* **11**, 1.

Echternach, M., Dippold, S., Sundberg, J., Arndt, S., Zander, M. F. and Richter, B. (2010). High-speed imaging and electroglottography measurements of the open quotient in untrained male voices' register transitions. *Journal of Voice* **24**, 644-650.

Elemans CPH, Spierts ILY, Hendriks M, Schipper H, Müller UK, van Leeuwen JL (2006) Syringeal muscles fit the trill in ring doves. *Journal of Experimental Biology* **209**: 965-977.

Elemans, C. P., Zaccarelli, R. and Herzel, H. (2008). Biomechanics and control of vocalization in a non-songbird. *J R Soc Interface* **5**, 691-703.

Elemans, C. P. H., Rasmussen, J. H., Herbst, C. T., During, D. N., Zollinger, S. A., Brumm, H., Srivastava, K., Svane, N., Ding, M., Larsen, O. N. et al. (2015). Universal mechanisms of sound production and control in birds and mammals. *Nat Commun* **6**.

Elemans, C. P. H., Spierts, I. L. Y., Müller, U. K., Leeuwen, J. L. v. and Goller, F. (2004). Superfast muscles control dove's trill. *Nature*, ***431***, 146.

Fee, M. S. and Scharff, C. (2010). The songbird as a model for the generation and learning of complex sequential behaviours. *ILAR journal* **51**, 362-377.

Fee, M. S., Shraiman, B., Pesaran, B. and Mitra, P. P. (1998). The role of nonlinear dynamics of the syrinx in the vocalizations of a songbird. *Nature* **395**, 67-71.

Goller, F. and Cooper, B. G. (2004). Peripheral motor dynamics of song production in the zebra finch. *Annals of the New York Academy of Sciences* **1016**, 130-152.

Goller, F. and Larsen, O. N. (1997a). *In situ* biomechanics of the syrinx and sound generation in pigeons. *J Exp Biol* **200**, 2165–2176.

Goller, F. and Larsen, O. N. (1997b). A new mechanism of sound generation in songbirds. *Proceedings of the National Academy of Sciences*, ***94***(26), 14787-14791.

Goller, F. and Riede, T. (2013). Integrative physiology of fundamental frequency control in birds. *Journal of Physiology-Paris* **107**, 230-242.

Gunter, H. E. (2003). *Mechanical stresses in vocal fold tissue during voice production* (Doctoral dissertation, Harvard University).

Hampala, V., Garcia, M., Švec, J. G., Scherer, R. C., & Herbst, C. T. (2016). Relationship between the electroglottographic signal and vocal fold contact area. *Journal of Voice*, *30*(2), 161-171.

Henrich, D. N. (2006). Mirroring the voice from Garcia to the present day: Some insights into singing voice registers. *Logopedics Phoniatrics Vocology* **31**, 3-14.

Herbst, C. T., Hampala, V., Garcia, M., Hofer, R., & Svec, J. G. (2017). Hemi-laryngeal Setup for Studying Vocal Fold Vibration in Three Dimensions. *Journal of visualized experiments. J. Vis. Exp.* ***129****, e55303.*

Herbst, C. T., Fitch, W. T. and Svec, J. G. (2010). Electroglottographic wavegrams: a technique for visualizing vocal fold dynamics noninvasively. *J Acoust Soc Am* **128**, 3070-8.

Herbst, C. T., Hess, M., Müller, F., Švec, J. G. and Sundberg, J. (2015). Glottal adduction and subglottal pressure in singing. *Journal of Voice* **29**, 391-402.

Herbst, C. T., Lohscheller, J., Svec, J. G., Henrich, N., Weissengruber, G. and Fitch, W. T. (2014). Glottal opening and closing events investigated by electroglottography and super-high-speed video recordings. *J Exp Biol* **217**, 955-63.

Herbst, C. T., Qiu, Q., Schutte, H. K. and Svec, J. G. (2011). Membranous and cartilaginous vocal fold adduction in singing. *J Acoust Soc Am* **129**, 2253-62.

Herbst, C. T., Schutte, H. K., Bowling, D. L. and Svec, J. G. (2017b). Comparing Chalk With Cheese—The EGG Contact Quotient Is Only a Limited Surrogate of the Closed Quotient. *Journal of Voice* **31**, 401-409.

Herbst, C. T., Svec, J. G., Lohscheller, J., Frey, R., Gumpenberger, M., Stoeger, A. S. and Fitch, W. T. (2013). Complex vibratory patterns in an elephant larynx. *J Exp Biol* **216**, 4054-64.

Herbst, C. T., Ternstrom, S. and Svec, J. G. (2009). Investigation of four distinct glottal configurations in classical singing--a pilot study. *J Acoust Soc Am* **125**, EL104-9.

Hess, M. M. and Ludwigs, M. (2000). Strobophotoglottographic transillumination as a method for the analysis of vocal fold vibration patterns. *Journal of Voice* **14**, 255-271.

Howard, D. M. (1995). Variation of electrolaryngographically derived closed quotient for trained and untrained adult female singers. *Journal of Voice* **9**, 163-172.

Howard, D. M., Lindsey, G. A. and Allen, B. (1990). Toward the quantification of vocal efficiency. *Journal of Voice* **4**, 205-212.

Ishizaka, K. and Flanagan, J. L. (1972). Synthesis of voiced sounds from a two-mass model of the vocal cords. *Bell Labs Technical Journal* **51**, 1233-1268.

Jensen, K. K., Cooper, B. G., Larsen, O. N. and Goller, F. (2007). Songbirds use pulse tone register in two voices to generate low-frequency sound. *Proc Biol Sci* **274**, 2703-10.

Jiang, J. J. and Titze, I. R. (1994). Measurement of vocal fold intraglottal pressure and impact stress. *Journal of Voice* **8**, 132-144.

Jing, B., Chigan, P., Ge, Z., Wu, L., Wang, S. and Wan, M. (2017). Visualizing the movement of the contact between vocal folds during vibration by using array-based transmission ultrasonic glottography. *The Journal of the Acoustical Society of America* **141**, 3312-3322.

Karakozoglou, S.-Z., Henrich, N., d'Alessandro, C. and Stylianou, Y. (2012). Automatic glottal segmentation using local-based active contours and application to glottovibrography. *Speech communication* **54**, 641-654.

Keller, G. B. and Hahnloser, R. H. (2009). Neural processing of auditory feedback during vocal practice in a songbird. *Nature* **457**, 187-90.

King, A. (1989). Functional anatomy of the syrinx. *Form and function in birds* **4**, 105-192.

Lã, F. M. and Sundberg, J. (2015). Contact quotient versus closed quotient: a comparative study on professional male singers. *Journal of Voice* **29**, 148-154.

Lohscheller, J. and Eysholdt, U. (2008). Phonovibrogram visualization of entire vocal fold dynamics. *The Laryngoscope* **118**, 753-758.

Markowitz, J. E., Liberti III, W. A., Guitchounts, G., Velho, T., Lois, C. and Gardner, T. J. (2015). Mesoscopic patterns of neural activity support songbird cortical sequences. *PLoS biology* **13**, e1002158.

Marler, P. R. and Slabbekoorn, H. (2004). Nature's music: the science of birdsong: Academic Press.

Paulsen, K. (1965). *Das Prinzip der Stimmbildung in der Wirbeltierreihe und beim Menschen: Mit 96 Abb. u. 10 Tab* (Doctoral dissertation).

Qiu, Q. and Schutte, H. K. (2006). A new generation videokymography for routine clinical vocal fold examination. *The Laryngoscope* **116**, 1824-1828.

Riede, T. and Goller, F. (2010). Functional morphology of the sound-generating labia in the syrinx of two songbird species. *J Anat* **216**, 23-36.

Riede, T., Suthers, R. A., Fletcher, N. H. and Blevins, W. E. (2006). Songbirds tune their vocal tract to the fundamental frequency of their song. *Proc Natl Acad Sci U S A* **103**, 5543-8.

Rothenberg, M. (1992). A Multichannel Electroglottograph. *Journal of Voice*, *6*(1), 36-43

Scherer, R., Druker, D. G. and Titze, I. R. (1988). Electroglottography and direct measurement of vocal fold contact area. *Vocal fold physiology: voice production, mechanisms and functions. New York: Raven*, 279-291.

Shau, Y. W., Wang, C. L., Hsieh, F. J., & Hsiao, T. Y. (2001). Noninvasive assessment of vocal fold mucosal wave velocity using color Doppler imaging. *Ultrasound in Medicine and Biology*, *27*(11), 1451-1460.

Story, B. H. (2002). An overview of the physiology, physics and modeling of the sound source for vowels. *Acoustical Science and Technology* **23**, 195-206.

Story, B. H. and Titze, I. R. (1995). Voice simulation with a body-cover model of the vocal folds. *The Journal of the Acoustical Society of America* **97**, 1249-1260.

Titze, I. R. (1980). Comments on the myoelastic-aerodynamic theory of phonation. *Journal of Speech, Language and Hearing Research* **23**, 495.

Titze, I. R. (1990). Interpretation of the Electroglottographic Signal. *Journal of Voice* **4**, 1-9.

Titze, I. R. (1994). principles of voice production. Englewood Cliff, NJ 07632: Prentice-Hall inc.

Titze, I. R. and Talkin, D. T. (1979). A theoretical study of the effects of various laryngeal configurations on the acoustics of phonation. *The Journal of the Acoustical Society of America* **66**, 60-74.

Van den Berg, J. (1958). Myoelastic-aerodynamic theory of voice production. *Journal of Speech, Language, and Hearing Research*, *1*(3), 227-244.

Verdolini, K., Chan, R., Titze, I. R., Hess, M. and Bierhals, W. (1998a). Correspondence of electroglottographic closed quotient to vocal fold impact stress in excised canine larynges. *Journal of Voice* **12**, 415-423.

Verdolini, K., Druker, D. G., Palmer, P. M. and Samawi, H. (1998b). Laryngeal adduction in resonant voice. *Journal of Voice* **12**, 315-327.

Zollinger, S. A. and Suthers, R. A. (2004). Motor mechanisms of a vocal mimic: implications for birdsong production. *Proceedings of the Royal Society of London B: Biological Sciences* **271**, 483-491.

Figures

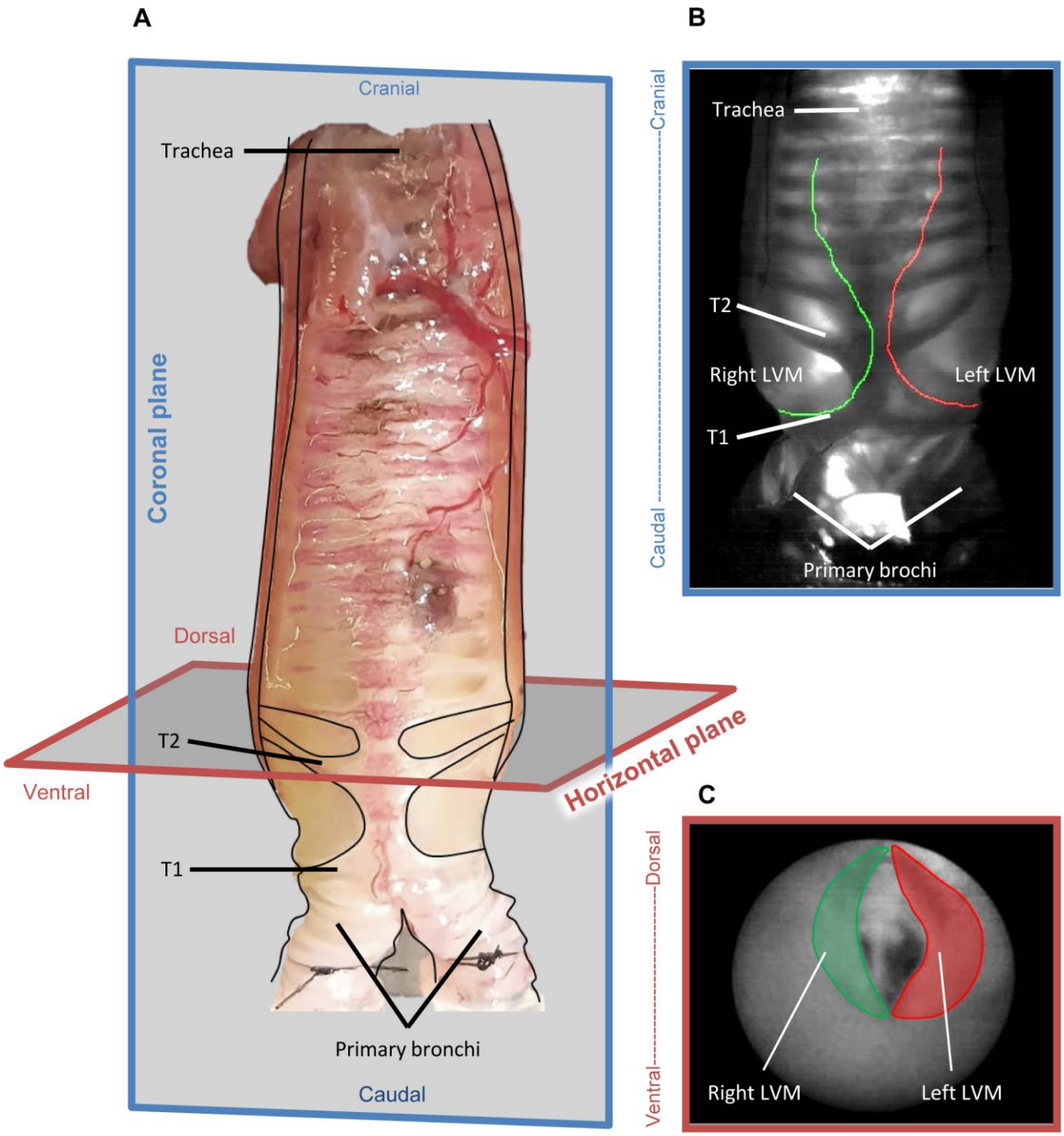

Figure 1. Syrinx morphology and imaging planes. (A) Ventral view of pigeon syrinx, T indicating trachea, TL Trachealateralis, and PG primary bronchi. The two planes used for examining kinematics, the coronal plane and the horizontal plane. (B) Transilluminated syrinx in the coronal plane with traced left (red) and right (green) LVM. (C) Tracheal view (i.e. horizontal plane) onto the left LVM (red) and the right (green) LVM.

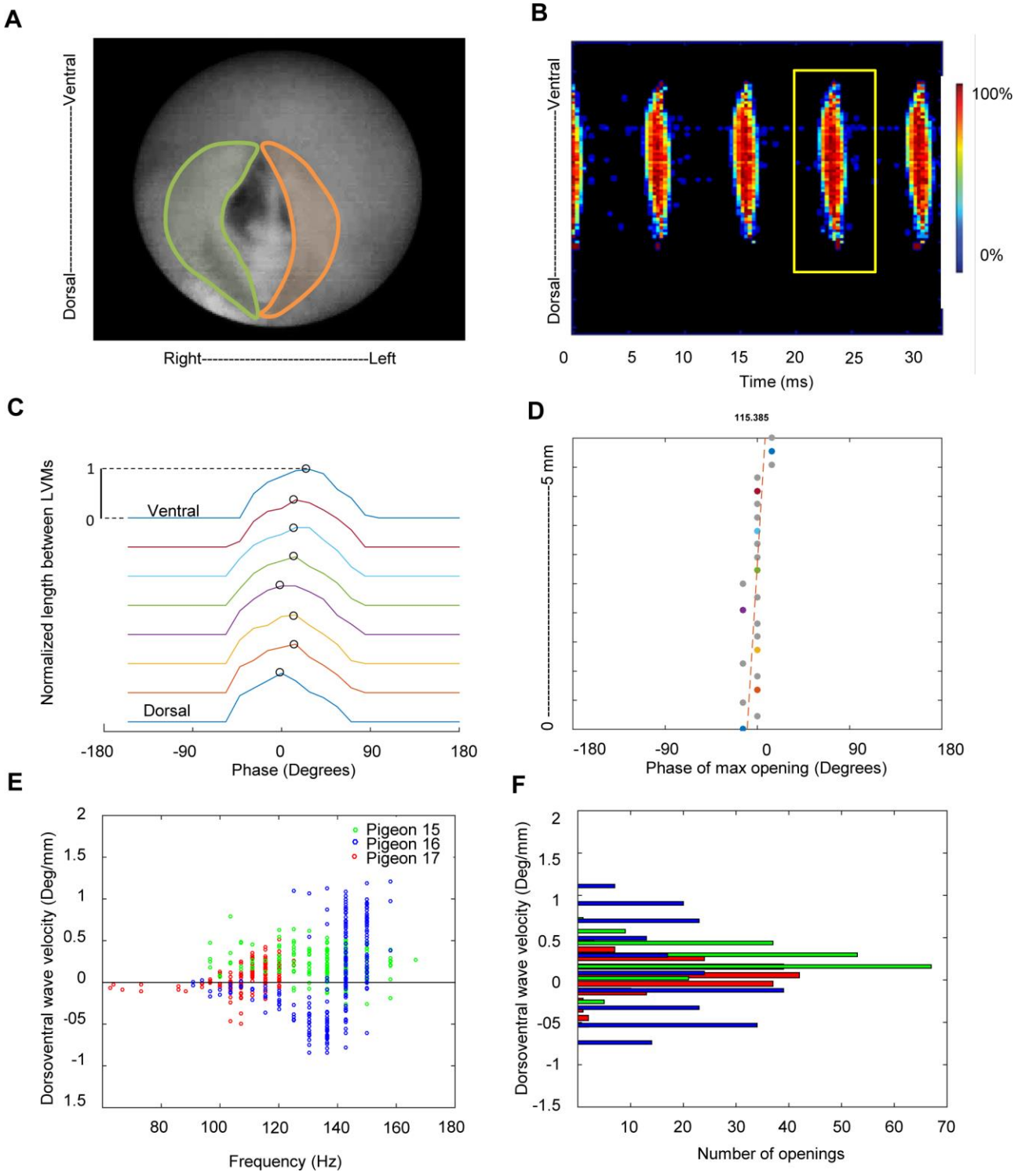

Figure 2. The pigeon syrinx does not exhibit dorsoventral oscillatory waves during self-sustained vibration in vitro. (A) Horizontal view of the two LVMs in the pigeon syrinx (right LVM green, left LVM orange) and the "glottal" opening between them filmed by a tracheal endoscope. (B) Glottovibrogram illustrating normalized opening as function of dorsoventral position and time**.** (C) Phase relation of glottal width on the dorsoventral axis relative to maximal LVM distance (i.e. maximal glottal width) at the midline. Only 8 different positions are shown here for clarity. (D) Phase of maximal LVM distance as a function of dorsoventral position for all 22 pixels of the glottis. Color-coding as in panel C. The slope of the linear regression (dashed red line) is the estimated wave speed *v*, which equals zero when no DV wave is present. (E) DV wave speed ***v*** as function of f_o of LVM vibrations in 588 opening/closing events in 3 animals showing a spread of the data as frequency increases. (F) Histogram of data in panel E showing that the data distribution for all three individuals: the mean is 0 deg/mm, and 95% of all values fall within a range of ±0.8 deg/mm.

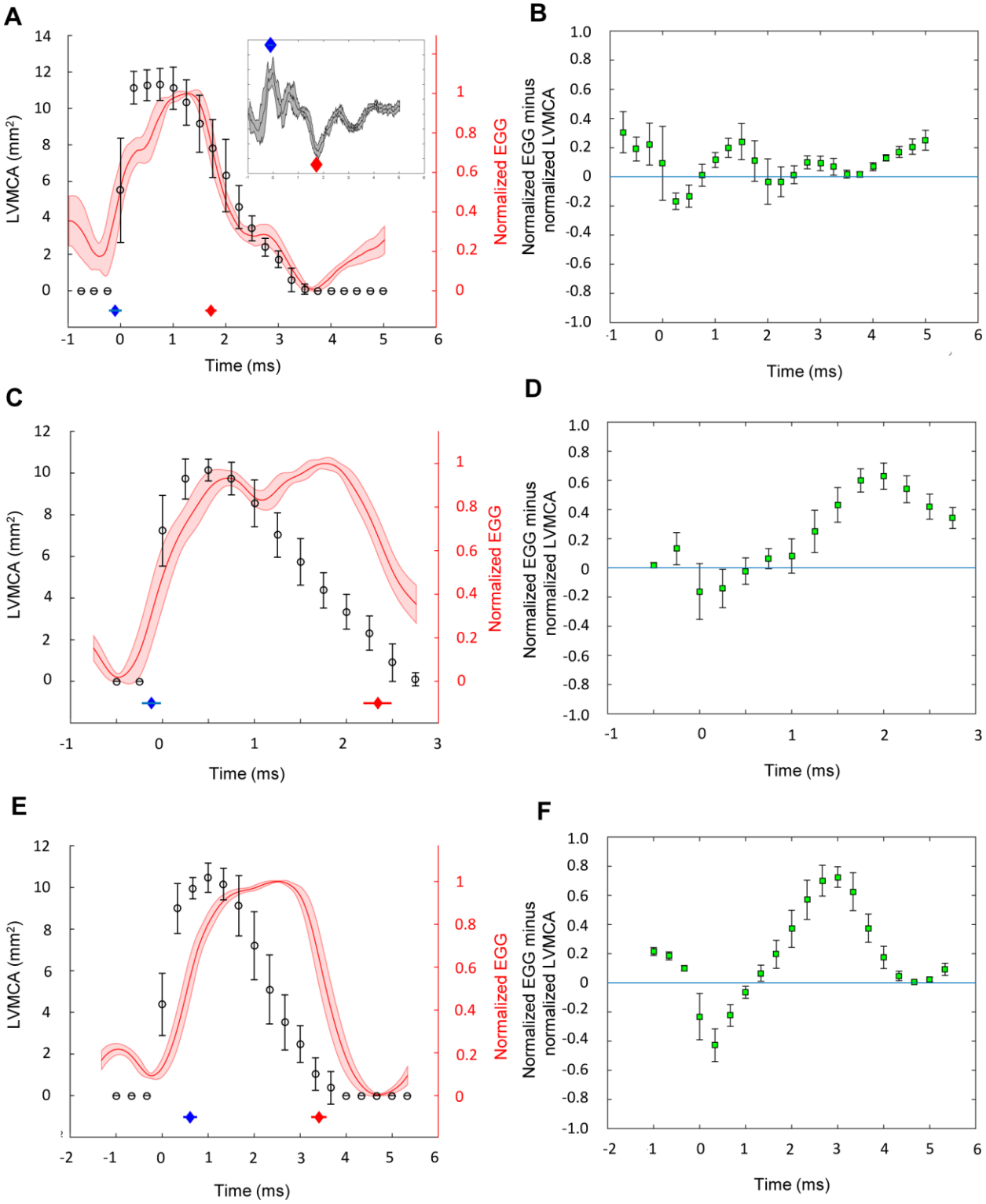

Figure 3. Within cycle vocal fold contact area and its relationship to EGG. (A,C,E) pLVMCA averaged over 10 consecutive cycles (black circles, mean ±std) and EGG (mean red line ±std shaded area). Also indicated are local maxima (blue dots, mean±std) and minima (red diamonds mean±std) of the dEGG signal. Time is indicated in ms after the first contact. The insert in A shows the corresponding dEGG waveform (arbitrary units) for this respective example, with diamonds indicating minima and maxima. (B,D,F) Normalized average difference between EGG and pLVMCA over the oscillatory cycle.

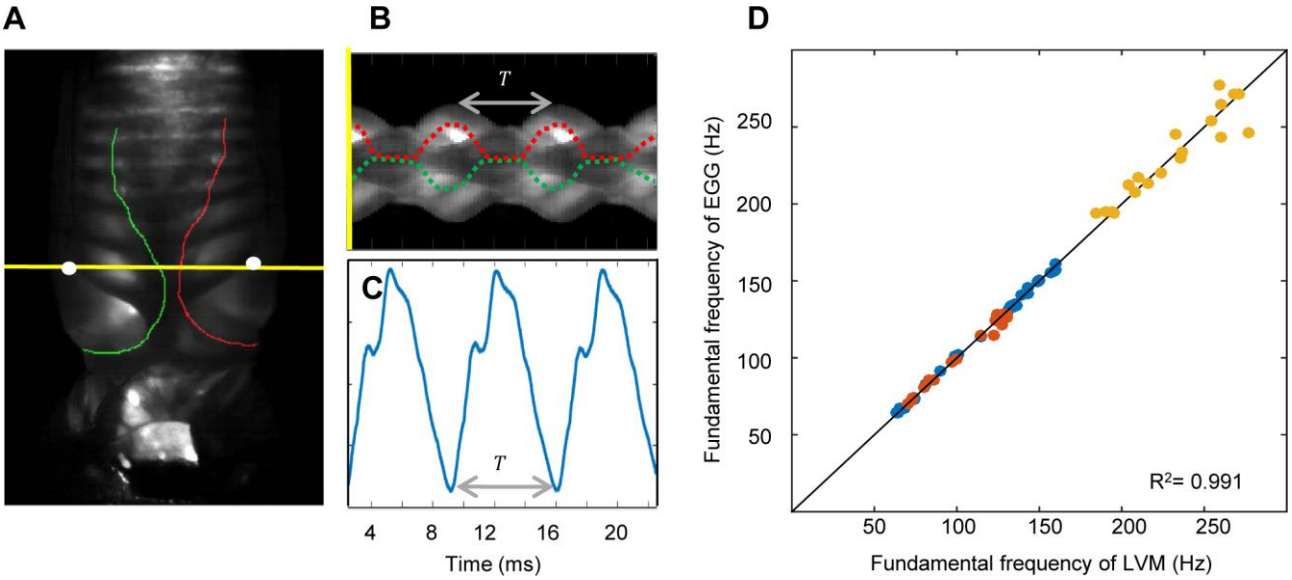

Figure 4. EGG accurately predicts the vibration frequency of the LVMs. (A) Coronal view of the syrinx using transillumination. The LVMs exhibit self-sustained vibrations during sound production. Inner LVM surface indicated by green (right) and red (left) lines. White dots indicate position of EGG electrodes. The yellow line indicates the position where a digital kymogram (DKG) was computed, shown in panel B. (B) Short segment of the DKG extracted at location indicated in panel A showing the motion of the LVMs inner surface over time. One period (T) of vibration is indicated and used to calculate the vibration frequency $f_o=1/T$. (C) EGG signal corresponding to the DKG in panel B. (D) Fundamental frequency of the EGG signal as a function of the observed vibration frequency of the LVM from a total of 72 vibratory cycles in three biological replicates. Individual regressions: slope = 0.9603, 0.9889 and 0.8786 and R^2=1.0, 1.0 and 0.8775 for the three animals, respectively.

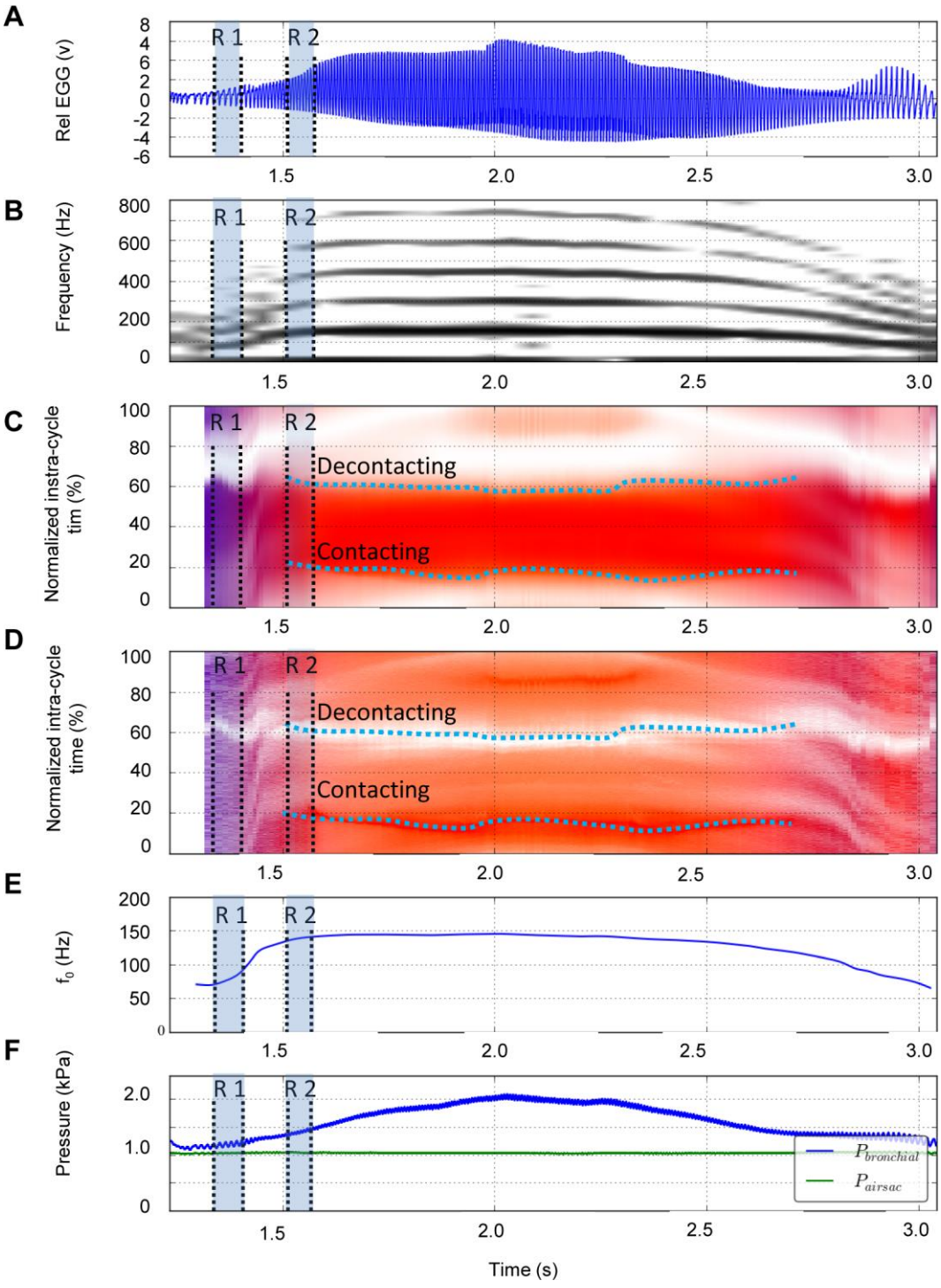

Figure 5 Development of the EGG signal during dynamic pressure excitation. (A) Oscillogram and (B) spectrogram of the EGG signal. R1 and R2 denotes regime 1 and 2 investigated in Fig 6. (C, D) Wavegrams of normalized EGG and dEGG cycles, respectively. (E) Fundamental frequency of the EGG signal. (F) Air sac pressure and bronchial air pressure.

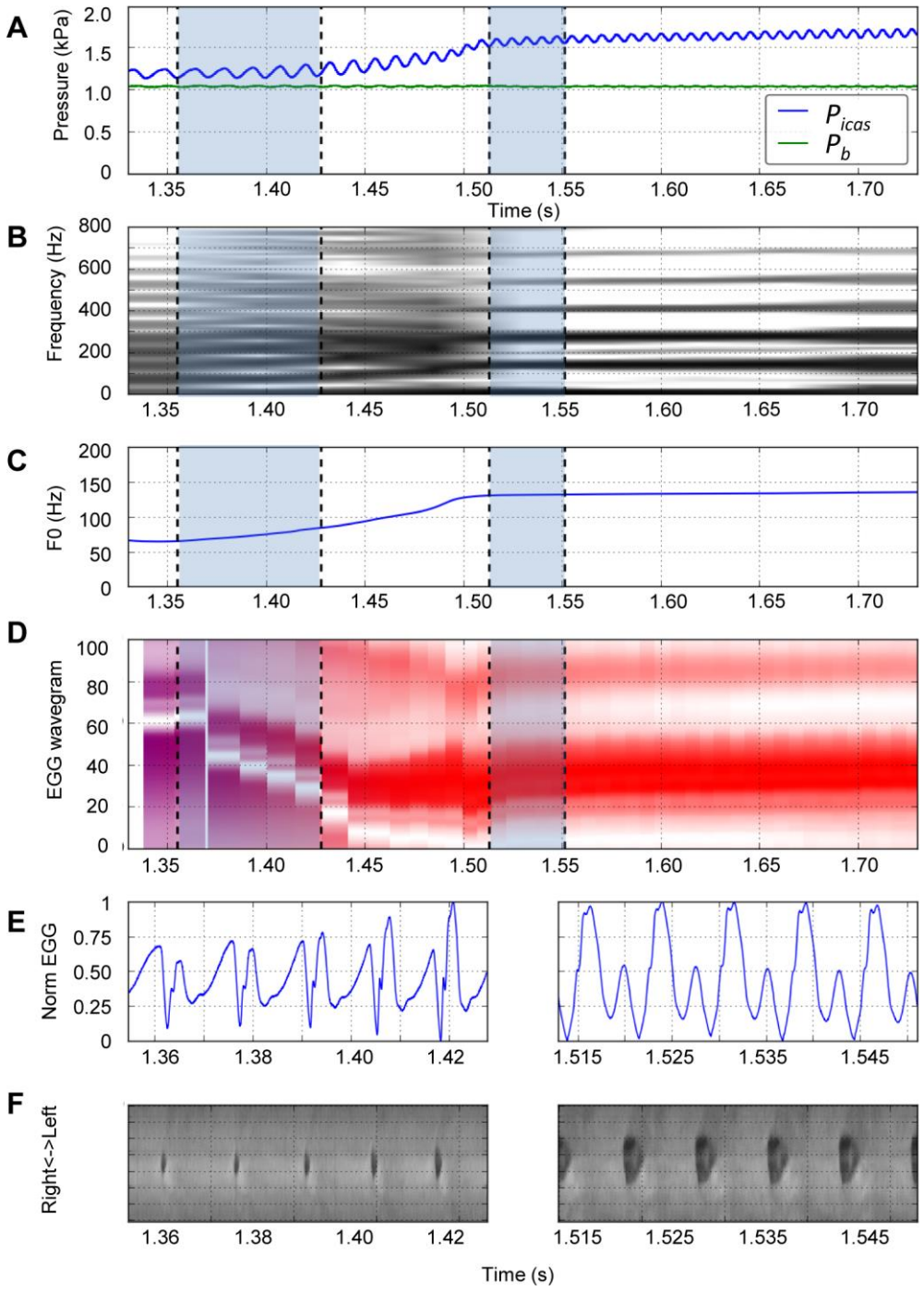

Figure 6. LVM dynamics confirm the presence of two distinct oscillatory modes as suggested by EGG signals. (A) The two driving pressures p_{icas} and p_b with the two time ranges indicated (shaded boxes) containing the two observed distinct vibratory modes. (B) Spectrogram of EGG signal showing distinct f_o ranges in the two marked time segments (C) f_o of EGG signal (D)

EGG wavegram showing a distinct shape change between the two time ranges, suggesting distinct vibratory modes. (E) EGG signal extracted at time offsets indicated in panels A-D. (F) VKG synchronized with EGG segments shown in panel E. The closed quotient is larger in first mode (0.94) as compared to second mode (0.72).